Hydrodynamics of Magnetic Fluids

Shinichi Kamiyama
Institute of Fluid Science, Tohoku University Katahira 2-1-1, Aobaku, Sendai, 980, Japan

Kazuo Koike
Tohoku Gakuin University, Chuo 1-13-1, Tagajo, Miyagi Prefecture, 985, Japan

Received September 2, 1994

A review is presented of the hydrodynamics of magnetic fluid research mainly conducted in Japan. The topics treated are various pipe flow problems and rheological characteristics of magnetic fluid in a strong magnetic field. First, the effect of uniform and nonuniform magnetic fields on steady pipe flow resistance is clarified. Then the oscillatory pipe flow characteristics in the application of stationary and nonstationally magnetic fields are investigated. Finally gas-liquid two-phase flow in a pipe is taken up. The experimental results suggest that the particles in a fluid partially aggregate in the applied magnetic field.

I. Basic equations of hydrodynamics

Magnetic fluids are well known to be a colloidal suspension of many fine particles of a solid ferromagnetic material in a carrier liquid such as water, hydrocarbon, ester and fluorocarbon. A most important feature is that the liquid that can respond to magnetic field. This characteristic results from the magnetic body force occuring in magnetic field.

1.1 Magnetic body force

The hydrodynamics of magnetic fluids differs from that of ordinary fluids by the inclusion of a magnetic stress tensor which is well known as the Maxwell stress tensor. If the local magnetization vector is collinear with the local magnetic field vector in any volume element, tlie following expression for the magnetic stress tensor in magnetic fluids can be obtained in the general form[1]:

$$\mathcal{T}_{ij} = -\left\{\mu_0 \int_0^H \left(\frac{\partial M v}{\partial v}\right)_{H,T} dH + \frac{\mu_0}{2} H^2\right\} \delta_{ij} + B_i H_j \,, \tag{1}$$

where M is magnetization, H is magnetic field, v is specific volume (m^3/kg), δ_{ij} is the Kronecker delta, and μ_0 is the permeability of free space and has the value 4π x $10^{-7} H/m$. In Cartesian coordinates, j is a component of the vectorial force per unit area, or traction, on an infinitesimal surface whose normal is oriented in i direction.

The magnetic body-force density is given by $f_m = \mathrm{V} \cdot \mathcal{T}$. Its components are represented by

$$f_j = (\nabla \cdot \mathcal{T})_j = \sum_i \frac{\partial \mathcal{T}_{ij}}{\partial x_i} \,. \tag{2}$$

The vector expression for the magnetic body force may be written as

$$f_m = -\nabla \left\{\mu_0 \int_0^H \left(\frac{\partial M v}{\partial v}\right)_{H,T} dH\right\} + \mu_0 (\mathbf{M} \cdot \nabla)\mathbf{H} \,. \tag{3}$$

1.2 Quasi-stationary hydrodynamics of magnetic fluids

To analyze magnetic fluid flow, it is necessary to formulate the momentum equation for magnetic fluids. A momentum equation of magnetic fluids was first proposed by Neuringer and Rosensweig[2]. They considered the limiting case that the relaxation time for magnetization is zero; that is, tlie magnetization M is collinear with the magnetic field H. Collinearity is a good approximation for sufficiently small size particles which behave superparamagnetically. The direction of M, then, rotates freely within the solid particle.

The system of hydrodynamic equations of magnetic fluids is described as follows: the continuity equation is

$$\frac{\partial \rho}{\partial t} + \nabla \cdot (\rho u) = 0 \ , \tag{4}$$

the equation of motion is

$$\rho \frac{Du}{Dt} = -\nabla p + \mu_0 (\mathbf{M} \cdot \mathrm{V}) \mathrm{H} - \nabla \rho g z + \eta \nabla^2 u \ , \tag{5}$$

the Maxwell equation is

$$\nabla \times \mathbf{H} = j \approx 0, \quad \nabla \cdot \mathbf{B} = 0 \ , \tag{6}$$

the equation of state is

$$p = p(\rho, T) \ , \tag{7}$$

and the equation of magnetization is

$$M = M_0(\rho, T, \mathrm{H}) \ . \tag{8}$$

Next, the energy equation is given by

$$\rho c \frac{DT}{Dt} + \mu_0 \left(\frac{\partial M}{\partial T} \right)_H \frac{DH}{Dt} = \nabla \cdot (\kappa \nabla T) + \Phi \ , \tag{9}$$

where c is the specific heat, κ the thermal conductivity and Φ the viscous dissipation energy.

The second term of the left-hand side of Eq.(9) expresses the heating due to the magnetocaloric effect of magnetic substance in a nonuniform magnetic field. The magnetic fluid is, therefore, heated by entering into the strong magnetic field region and cooled by outgoing from it. Equations (4)-(9) compose a system of quasi-stationary hydrodynamic equations of magnetic fluid.

Now, we must consider the existence of jump boundary conditions as an additional feature in concert since it is crucial to the magnetic fluid flow. Let us consider an element of the surface at a boundary between two different media as illustrated in Fig. 1. From Eq.(1), the traction on a surface element with unit normal n is

$$n \cdot \mathcal{T}_{ij} = -n \left(\mu_0 \int_0^H \frac{\partial M v}{\partial v} dH + \frac{\mu_0}{2} H^2 \right) + \backslash \cdot \mathbf{BH} \ . \tag{10}$$

The difference of this magnetic stress across an interface between media is a force oriented along the normal which may be expressed as

$$[n \cdot \mathcal{T}] = n[\mathcal{T}_{nn}] = n \left(\mu_0 \int_0^H \frac{\partial M v}{\partial v} dH + \frac{\mu_0}{2} M_n^2 \right) \ . \tag{11}$$

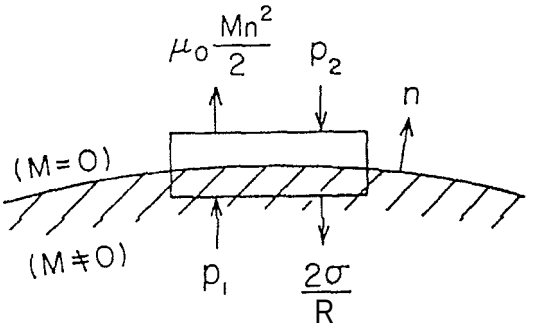

Figure 1: Balance of forces in the boundary condition.

The square brackets denote difference between the quantities across the interface and subscript n denotes the normal direction.

When the contacting media are both fluids, the stress difference, from Eq.(10), may be balanced by actual thermodynamic pressure $p(\rho, \mathrm{T})$. If one medium is nonmagnetic, the following result is obtained:

$$p^* = p_0 - \left(\frac{\mu_0}{2} \right) M_n^2 + \frac{2\sigma}{R} \ , \tag{12}$$

where p_0 is the pressure in the nonmagnetic fluid medium, R is the radius of curvature of the surface and σ is the surface tension.

1.3 Treatment as Micropolar fluids

If a magnetic fluid includes relatively large particles, the relaxation time for magnetization of the fluid is determined by Brownian rotation. In this case, the particles can be considered as rigid magnetic dipoles; that is, one can assume that the magnetic moment of a particle changes its orientation only for rotation of the particle itself. Then, the presence of an externa1 magnetic field results in the prevention of the rotation of the particle and in the appearance of the mechanism of rotational viscosity. The existence of rotational viscosity leads to an increase in the effective viscosity of the fluid.

To explain the dependence of the viscosity on a magnetic field, let us consider the motion of an individual spherical particle in a homogeneous shear stream $\Omega = (1/2)\nabla \times \Pi = \text{const.}$, planar Couette flow[3] as

sketched in Fig. 2. In the absence of the field, the particle's angular velocity w equals to Ω. However, in a magnetic field, the particle is acted on by the magnetic torque $\mu_0 \mathbb{I} \times \mathrm{H}$, which changes the state of its rotation. As a result, a frictional-force torque of $\pi d^3 \eta_0 (\Omega - \mathrm{w})$ which is the mechanism of the rotational-viscosity, is produced

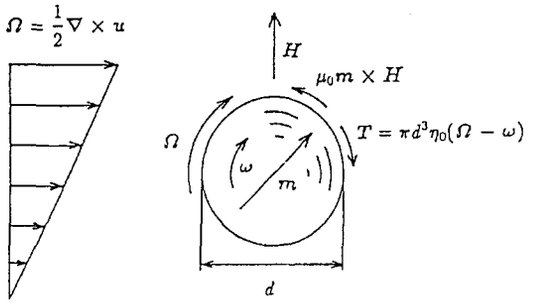

Figure 2: Motion of spherical particle in a homogeneous shear stream.

In the hydrodynamic description of a suspension as a homogeneous medium, it is necessary to treat it as a fluid having internal angular momentum. The volume density of internal angular momentum is denoted by

$$\mathbf{S} = I\omega \ . \tag{13}$$

Here $\mathbf{I} = 8\pi r^5 \rho_S n/15$ is the sum of moments of inertia of the spheres per unit volume and w the angular velocity of their ordered rotation.

For a liquid with internal rotation, the laws of momentum and angular-momentum conservation are expressed as follows[4]:

$$\begin{aligned} \rho \frac{Du}{Dt} &= -\nabla p + \eta \nabla^2 u + \mu_0 (\mathbf{M} \cdot \nabla)\mathbf{H} \\ &+ \frac{1}{2\tau_S} \nabla \times (\mathrm{S} - \mathrm{IQ}), \end{aligned} \tag{14}$$

$$\frac{D\mathbf{S}}{Dt} = \mu_0 (\mathbf{M} \times \mathbf{H}) - \frac{1}{\tau_S}(\mathbf{S} - I\Omega) + \gamma \nabla^2 \mathbf{S} \ . \tag{15}$$

Here $\gamma = 2r^2/(3\tau_B)$ is the diffusion coefficient, $\tau_S = r^2 \rho_S/(15\eta_0)$ is relaxation time of particle rotation and $I/(2\tau_S)$ means the rotational viscosity. To obtain a closed system of equations, it is necessary to add the equation for $D\mathbf{M}/Dt$ to the system (14), (15); that is,

$$\frac{\mathrm{D\,M}}{Dt} = \frac{\mathbf{S} \times \mathbf{M}}{I} - \frac{\mathbf{I}}{\tau_B}\left(\mathbf{M} - M_0 \frac{\mathbf{H}}{|H|}\right) \ , \tag{16}$$

where τ_B is relaxation time of Brownian motion, and M_0 the equilibrium magnetization of magnetic fluid. Equations (4), (6)-(9) and (14)-(16) form a complete system of equations.

II. Pipe flow problems

Pipe flow problems of magnetic fluids in an applied magnetic field are very important not only as the basic studies of hydrodynamics of magnetic fluid, but also as the problems related closely to the development of applied devices such as new energy conversion system, magnetic fluid damper and actuator.

II.1 Theoretical analysis of steady laminar flow

II.1.1 Flow in an axial magnetic field

First, let us consider the steady laminar pipe flow in an axial magnetic field $H_z(z)$ and apply the basic equations derived in Section 1.3 as the micropolar fluid of this problem[5]. If the particle radius is on the order of 10^{-8}m, then the values of τ_S become the order of 10^{-11}s and hence the l.h.s. and the 3rd term in the r.h.s. of Eq.(15) may be neglected. Therefore, eliminating S from Eqs.(14), (15) and (16), equation (14) reduces to

$$\frac{dp}{dz} = \eta \frac{1}{r}\frac{d}{dr}\left(r\frac{du_z}{dr}\right) + \mu_0 M_z \frac{dH_z}{dz} - \frac{\mu_0}{2r}\frac{\partial}{\partial r}(r M_r H_z) \ . \tag{17}$$

Also, the following relations are obtained:

$$M_r = \frac{\Omega \tau_B M_z}{1 + \mu_0 \tau_S \tau_B M_z H_z / I} \tag{18}$$

and

$$u_z \frac{\partial M_z}{\partial z} = \frac{1}{\tau_B}\left\{ M_0 - M_z - \frac{(\Omega\tau_B)^2 M_z}{(1 + \mu_0 \tau_S \tau_B M_z H_z/I)^2} \right\} \ . \tag{19}$$

Here the equilibrium magnetization M_0 is assumed to be expressed by the Langevin function L; that is,

$$M_0 = nmL(\xi) \ . \tag{20}$$

where $\mathrm{L}() = \coth\xi - \xi^{-1}$, $\xi = \mu_0 mH/kT$. In the case of a uniform magnetic field, the second term in the r.h.s. of Eq.(17) and the l.h.s. of Eq.(19) vanish[6].

(1) Solution in the case $\Omega\tau_B << 1$

If the condition that the rotary Péclet number $P_{er} = 2\Omega\tau_B << 1$ holds, the following relation is obtained from Eq.(19).

$$M_z \approx M_0 \ . \tag{21}$$

Now, let's introduce the following dimensionless quantities:

$$\left.\begin{array}{lll} r^* = r/r_0, & z^* = z/r_0, & u_z^* = u_z/u_0 \\ h^* = H_z/H_{max}, & M_z^* = M_z/M_{0max}, & p^* = pr_0/(\eta u_0) \\ L^* = L(\xi)/L(\xi_{max}), & A = \mu_0\tau_S\tau_B H_{mx}M_{0max}/I & \end{array}\right\} \tag{22}$$

Here r_0 is the pipe radius and u_0 is the mean flow velocity. Then, Eq. (17) is expressed as

$$\frac{d}{dz}\left\{p^* - \frac{r_0 nkT}{}\ln(\xi^{-1}\sin\xi)\right\} = \frac{2}{r^*}\left(1+\frac{\Delta\eta}{\eta}\right)\frac{du_z^*}{dr*} \ , \tag{23}$$

where

$$\Delta\eta = \frac{3}{2}\varphi\eta_0\frac{\mathrm{Ah^*L^*}}{1+Ah^*L^*} \ , \tag{24}$$

$\varphi = (4/3)\pi a^3 n$ is volumetric concentration of particles and a is the particle radius.

Applying tlie boundary condition $u_z^* = 0$ at r* = 1 to Eq.(23), we obtain the solution as

$$u_z^* = \frac{dp^{*'}/dz^*}{4(1+\Delta\eta/\eta)}(r^{*2}-1) \ , \tag{25}$$

where

$$p^{*'} = p^* - \frac{r_0 nkT}{\eta u_0}\ln(\xi^{-1}\sinh\xi) \ . \tag{26}$$

Eq. (25) shows that the flow is a Poiseulle one of a Newtonian fluid whose apparent viscosity is $\eta_e = \eta + \Delta\eta$. Applying the continuity equation, the velocity profile is also represented by

$$u_z^* = 2(1-r^{*2}) \ , \tag{27}$$

Integrating Eq.(23), tlie pressure difference between arhitrary two points z_1^* and z_2^* in the applied field region is given by

$$p_1^* - p_2^* = -\frac{r_0 nkT}{\eta u_0}|\ln(\xi^{-1}\sinh\xi)|_{z_1^*}^{z_2^*} + 8(z_2^*-z_1^*) + 8\int_{z_1^*}^{z_2^*}\frac{\Delta\eta}{\eta}dz^* \ . \tag{28}$$

The first term of r.h.s. of Eq.(28) means that tlie static pressure difference due to the magnetic body force; the 2nd and 3rd terms correspond to the pressure drop due to friction loss without magnetic field and additional loss with magnetic field, respectively.

(2) Solution the case $\Omega\tau_B \sim 1$

It is very difficult to solve Eq.(19) generally in the case of $P_{er}(= 2\Omega\tau_B) \sim 1$. However, the left-hand side of Eq.(19) becomes small in the region near the pipe wall where the effects of angular velocity of fluid R is large. On the other hand, R N 0 in the central region of the pipe and hence the magnetization M_z may be considered as M_z N M_0. Now, we put

$$M_z^*(r^*, z^*) = M_0^*(z^*)\delta(r^*, z^*) \tag{29}$$

and consider the method to obtain the distribution of $\delta(r^*, z^*)$ approximately. Neglecting the term of $(d\delta/dz^*)$ and assuming u_z^* to be Eq.(27), Eq. (19) reduces to

$$[\mathrm{i} - \delta\{\mathrm{i} + \frac{2u_0\tau_B}{r_0}(1-r^{*2})\frac{\omega}{\mathrm{dz^*}}\ln L^*(\xi)\quad (1+Ah^*L^*\delta)^2 = (\Omega\tau_B)^2\delta \ . \tag{30}$$

The radial distribution of 6 at each section z^* can be calculated from Eq. (30). Eq. (17), in the case of $P_{er} \sim 1$, becomes

$$\frac{du_z^*}{dr^*} = \frac{r^*}{2(1+\Delta\eta/\eta)} \left\{ \frac{dp^*}{dz^*} - \frac{r_0 \mu_0 M_{0max} H_{max}}{\eta u_0} \delta L^*(\xi) \frac{dh^*}{dz^*} \right\} , \tag{31}$$

where

$$\Delta\eta = \frac{3}{2}\varphi\eta_0 \frac{\text{Ah*L*6}}{1 + Ah^* L^* \delta} . \tag{32}$$

It is clear from Eqs.(31) and (32) that the apparent viscosity depends on the flow shear rate R; that is, the magnetic fluid shows the non-Newtonian fluid property.

II.1.2 Flow in a transverse magnetic field

Next, we would like to present the steady laminar pipe flow in a transverse magnetic field as shown in Fig. 3[7]. The basic equations derived in Section 1.3 are applied to this problem, too. According to a consideration similar to the steady flow in an axial magnetic field mentioned before section, Eq. (14) reduces to

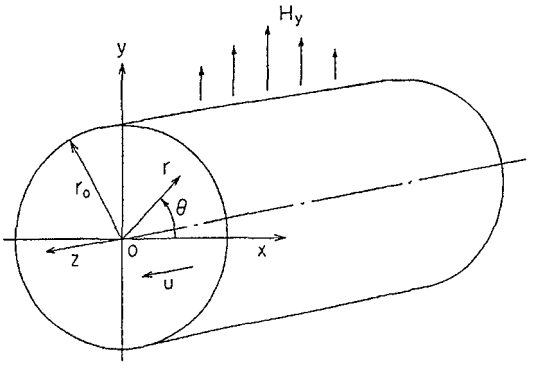

Figure 3: Steady pipe flow in a nonuniform transverse magnetic field.

$$\frac{dp}{dz} = \eta \frac{1}{r}\frac{d}{dr}\left(r\frac{du_z}{dr}\right) + \mu_0(M_r \sin\theta + M_\theta \cos\theta)\frac{dH_y}{dz} + \frac{\mu_0}{2} H_y \left(\sin\theta \frac{\partial M_r}{\partial r} + \cos\theta \frac{\partial M_z}{r\partial\theta}\right) . \tag{33}$$

(1) Solution in the case $\Omega\tau_B \ll 1$

The following relations are obtained from Eq.(15) in the case of $P_{er} = 2\Omega\tau_B \ll 1$:

$$M_r = M_0 \sin\theta , \quad M_\theta = M_0 \cos\theta \tag{34}$$

and

$$M_z \cong -\Omega\tau_B \frac{M_0 \sin\theta}{1 + \mu_0 \tau_S \tau_B M_0 H_y / I} . \tag{35}$$

Now, let's introduce the same dimensionless quantities as for the flow in axial magnetic field except for h* = H_y/H_{max}. Then, Eq. (33) is expressed as

$$\begin{aligned} \frac{d}{dz^*}\left\{ p^* - \frac{r_0 nkT}{\eta u_0} \ln(\xi^{-1}\sinh\xi) \right\} &= \left(1 + \sin^2\theta \frac{2\Delta\eta}{\eta}\right) \frac{d^2 u_z^*}{dr^{*2}} \\ &+ \left(1 + \cos^2\theta \frac{2\Delta\eta}{\eta}\right) \frac{du_z^*}{r^* dr^*} , \end{aligned} \tag{36}$$

where

$$\Delta\eta = \frac{3}{4}\varphi\eta_0 \frac{\text{Ah*L*}}{1 + Ah^* L^*} . \tag{37}$$

The increase in the apparent viscosity $\Delta\eta$ in a transverse magnetic field is just half of that in a longitudinal magnetic field (Eq.(32))[8].

Applying the boundary condition of $u_z^* = 0$ at $r^* = 1$ to Eq.(36), we obtain the same expressions for u_z^* and $p^{*'}$ as Eqs.(25) and (26), respectively. Thus, in the case of transverse magnetic field, it is shown that the flow is a Poiseulle one of a Newtonian fluid whose apparent viscosity is $\eta_e = \eta + \Delta\eta$, too. The pressure difference between arbitrary two points z_1^* and z_2^* in the applied field region is given by the same equation as Eq.(28).

(2) Solution in the case $\Omega\tau_B \sim 1$

In this case, the approximate procedure based on the same consideration as for the flow in the axial field is adopted to solve the equations. That is,

$$M^* = M/M_{0max}$$

and

$$M_y^* = M_0^*(z^*)\delta(r^*, \theta, z^*) = L^*\delta \ , \qquad (38)$$

the following relations are obtained from Eq.(14)-(16):

$$(1-\delta)(1+Ah^*L^*\delta)^2 = (\Omega\tau_B)^2(\delta - \cos^2\theta) \qquad (39)$$

and

$$\Delta\eta = \frac{3}{4}\varphi\eta_0\frac{Ah^*\mathrm{L}^*6}{1+Ah^*L^*\delta} \ . \qquad (40)$$

It is clear from Eqs.(39) and (40) that the apparent viscosity depends on the flow shear rate R, too.

11.2 Pipe flow resistance in laminar and turbulent flow

It is well known that the velocity profile of the fully developed laminar flow is parabolic in an ordinary Newtonian fluid. Then, the pressure drop is determined by the pipe friction coefficient λ as a function of Reynolds number Re : $\lambda = 64/Re$. Here, $Re = \rho u_0 d/\eta$. Experimental studies of the flow in an axial magnetic field were carried out using similar technique to ordinary fluid[5,6]. Fig. 4 shows the layout of the experimental apparatus to study the flow in an axial magnetic field. The open loop shown in this figure as L_1 was utilized in the case of low flow velocity. The flow rate was controlled by varying the position of upper reservoir R_1 and was measured by means of a weight tank. On the other hand, the closed loop L_2 was employed to perform the measurement at much higher Reynolds number. In this experiment, a copper tube of 6 mm in inner diameter was used. The test fluid was made by diluting Ferricolloid W-35 to mass concentrations of 20% and 25% with distilled water. The pressure difference between the upstream and clownstream pressure taps was measured by the manometer and the increasing rate of pipe friction coefficient λ was determined. Fig. 5 shows an example of the experimental results in the case of uniform magnetic field. In the cases of axial magnetic field, good agreement has been found between the experimental and predicted results concerning the increasing rate of the pipe friction coefficient. However, the decrease in the increasing rate is also observed at relatively high Reynolds number in the laminar flow regime; that is, the apparent viscosity depends on the angular velocity. If a correction parameter o is introduced into the term $\Omega\tau_b$ in Eq.(39) as $\alpha'\Omega\tau_b = \alpha\Omega \sim 1$ and the modified coefficient β is considered for the moment of inertia of particles as $\mathbf{I} = 8\beta\pi a^5\rho_s N/15$ (where the values of $\beta = 1.5$ and $\alpha = (2 \sim 3) \times 10^{-3}$s are taken as the appropriate ones in the modification of the basic equations), the experimental results can be explained qualitatively by the approximate analysis. The increasing rate for the turbulent flow is not so high compared with that for the laminar flow.

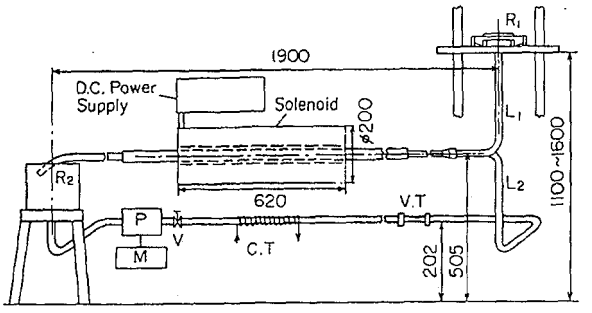

C.T: cooling tube, M: motor, P: pump, R_1: upper reservoir, R_2: lower reservoir, V: ball valve, V.T: venturi tube

Figure 4: Layout of experimental apparatus of pipe flow in the case of axial magnetic field.

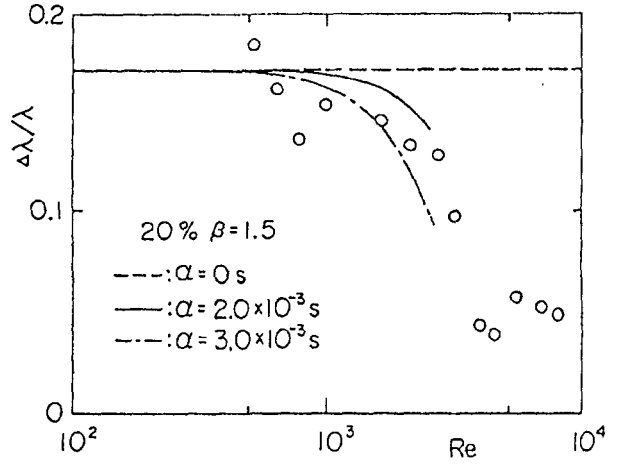

Figure 5: Experimental result of the increase rate of resistance coefficient.

On the other hand, some experimental studies of pipe flow in uniform and nonuniform transverse magnetic field have been carried out to clarify the effect of the field on the resistance in a wide range of Reynolds numbers for water- based and kerosene-based magnetic fluids[9−12]. One of them was carried out using experimental apparatus sketched in Fig. 6. The flow was driven by the rotary pump **(3).** The reservoir (5) is attached to the outlet of the pump to reduce the pulsation of the flow. The test section is located along the center line of the poles of an electromagnet. A magnetic field was applied transversely to the flow direction with the electromagnet. Fig. 7 shows the details of the test pipe and the magnetic field distribution along the axial direction of the pipe, where **I** means a current supplied to the electromagnet. The pipe is made of phenolic resin: the inner diameter is about 9.8mm. Twelve pressure taps are installed along the pipe axis as indicated in this figure. Typical experimental results are sketched in Fig. 8. It is clearly indicated in this figure that the pressure increases with the field strength H in the entrance region of magnetic field, due to the magnetic body force, and decreases in the outlet one. Moreover, the pressure drop caused by friction loss is larger in an applied magnetic field than in no magnetic field. The true pressure distribution shows the profile as indicated by solid line in this figure. However, if the pressure in the magnetic field region is measured by a manometer outside the magnetic field, the pressure difference in the manometer indicates only the pressure drop due to pipe friction loss as shown by chain line. In such a case, the magnetic force acts on the fluid in the connecting tube across the magnetic field and cancels the magnetic static pressure in the pipe. It is clear from the experimental data that there exists a large pressure drop in the nonuniform field region. Then, we would like to go into some detail on the pressure distribution measured by the manometer. As an example of experimental results in the case of water-based fluid, the pressure coefficient C_p along the pipe axis is plotted in Fig. 9. In this case,

$$C_p = \frac{\mathrm{P} - \mathrm{Pl}}{\rho u_0^2/2},$$

where p_1 means the pressure at the tap No.1 in Fig. 7. The pressure drop increases with the applied magnetic field strength; in particular, large pressure drop occurs in nonuniformfield regions, in particular at downstream of the pole piece. Measurements of the flow resistance were also made for another pipes with variable cross sectional area such as venturi tubes and long orifice[12]. It is shown in the experiment that a peculiar pressure drop occurs at the edges of the imposed magnetic field.

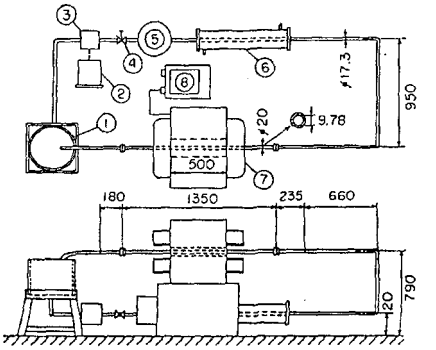

①Reservoir 1, @Motor, ③Pump, ④Valve, ⑤Reservoir 2, ⑥Cooling pipe, ⑦Electromagnet, ⑧D.C. power supply

Figure 6: Scheme of the experimental apparatus of pipe flow in the case of transverse magnetic field.

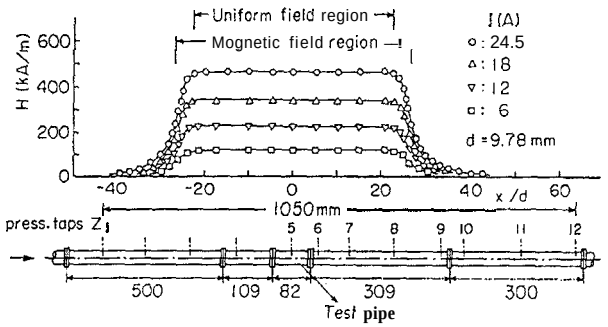

Figure 7: Distribution of the transverse magnetic field strength.

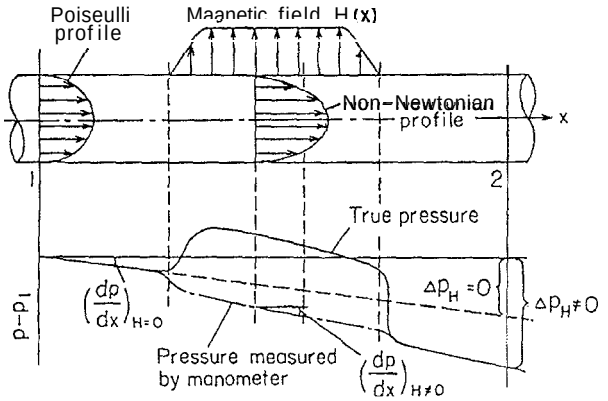

Figure 8: Pressure distribution along the pipe axis.

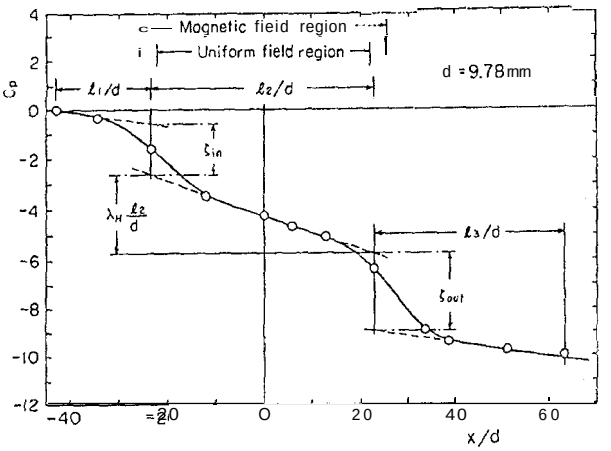

Figure 9: Explanation of the pressure drop under the applied magnetic field.

As a result, the pressure drop within the magnetic field is divided into three parts as sketched in Fig. 9. The following loss coefficients may be defined from the figure:

$$\zeta = \lambda_0 \frac{l_1+l_3}{d} + \lambda_H \frac{l_2}{d} + \zeta_{in} + \zeta_{out} , \qquad (41)$$

where λ_H denotes the resistance coefficient in uniform magnetic field and λ_0 in the absence of field. ζ_{in} and ζ_{out} are loss coefficients in nonuniform magnetic field regions at the inlet and outlet. Since tlie pressure gradient is supposed to be nearly constant in the uniform field region, the resistance coefficient λ_H was estimated. The relation hetween the resistance coefficient A, which corresponds to λ_H, and the modified Reynolds number Re^* is sliown in Fig. 10. The coefficient of pipe resistance λ and modified Reynolds number Re^* in this figure are defined

$$\lambda = \frac{64}{Re^*} \quad \text{and} \quad Re^* = \frac{\rho u_0 d}{\eta + \Delta\eta} . \qquad (42)$$

It is indicated in this figure that in the laminar flow regime the resistance coefficient λ increases with tlie supply current **I,** that is, with tlie intensity of magnetic field. In particular, the coefficient λ for water-based fluid is much larger than that for kerosene-hased fluid. On the other hand, λ for turbulent flow is not supposed to he influenced hy the application of magnetic field; it has a slightly lower value compared to the Blasius formula as a Newtonian fluid.

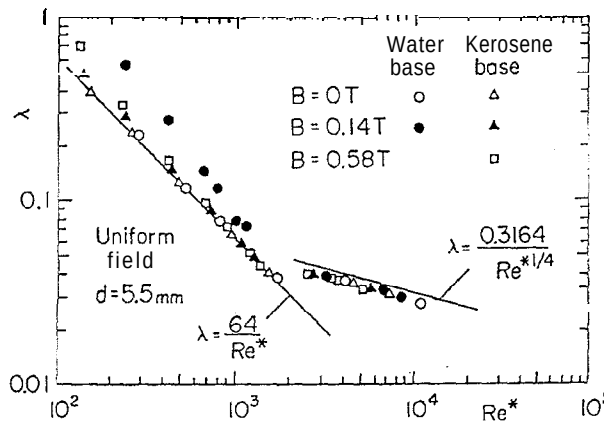

Figure 10: Effect of magnetic field strength on tlie relation of the resistance coefficient λ versus the Reynolds number Re in uniform magnetic field.

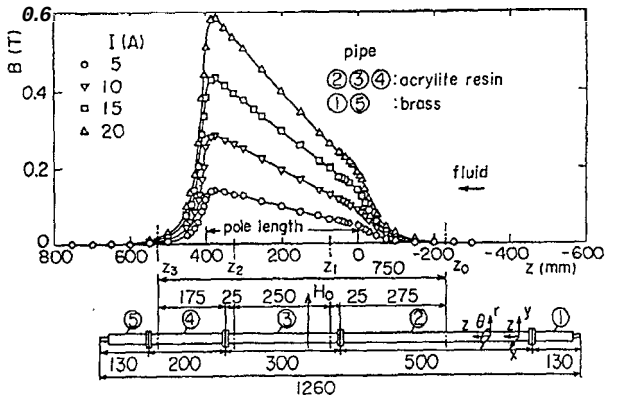

Figure 11: Distribution of the magnetic flux density in the test section.

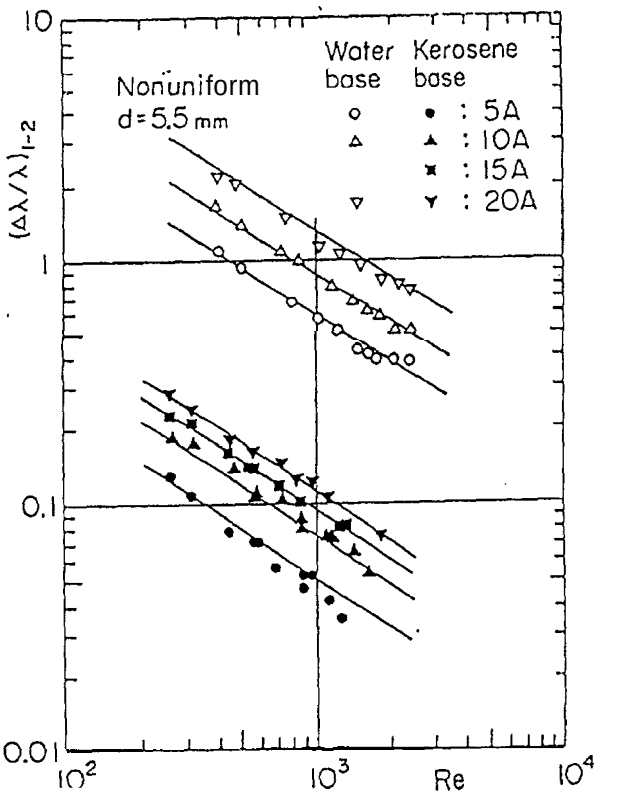

Figure 13: Increase rate of the resistance coefficient due to the magnetic field.

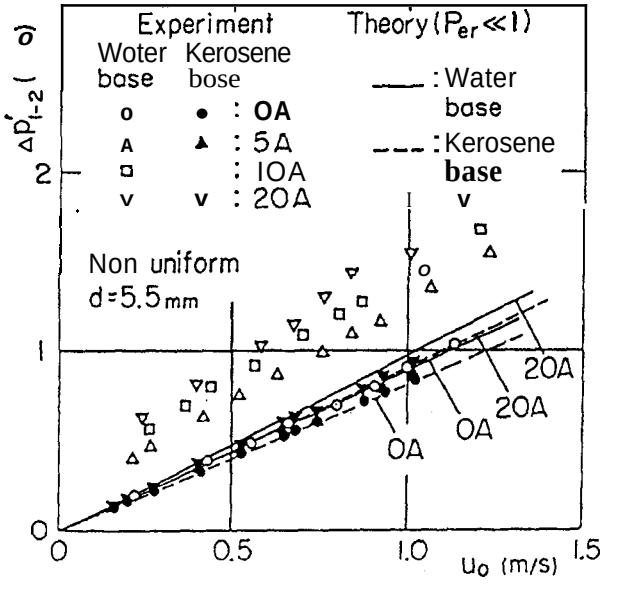

Figure 12: Pressure difference as a function of the mean flow velocity.

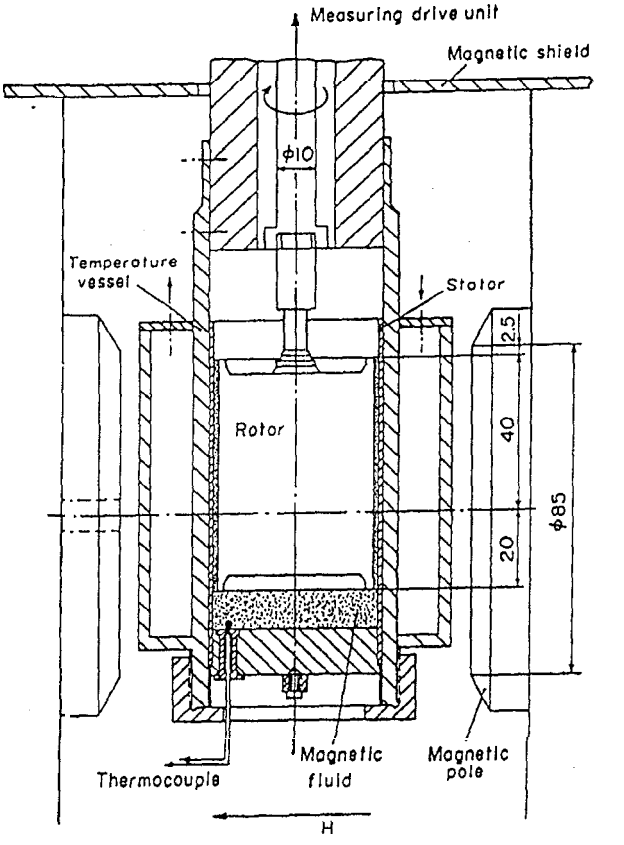

Figure 14: Scheme of the experimental apparatus of the modified concentric-cylinder-type viscometer.

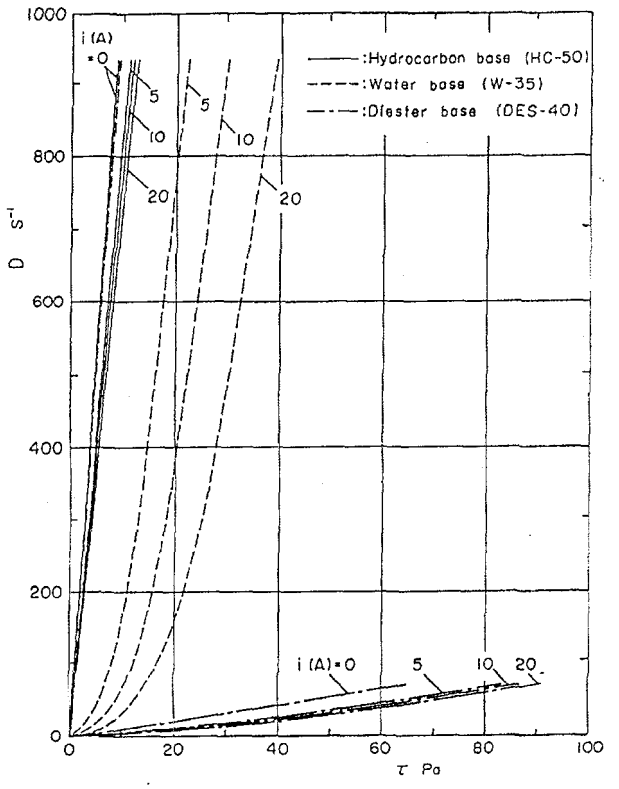

Figure 15: Rheological characteristics of the magnetic fluid (D: shear rate, r: shear stress).

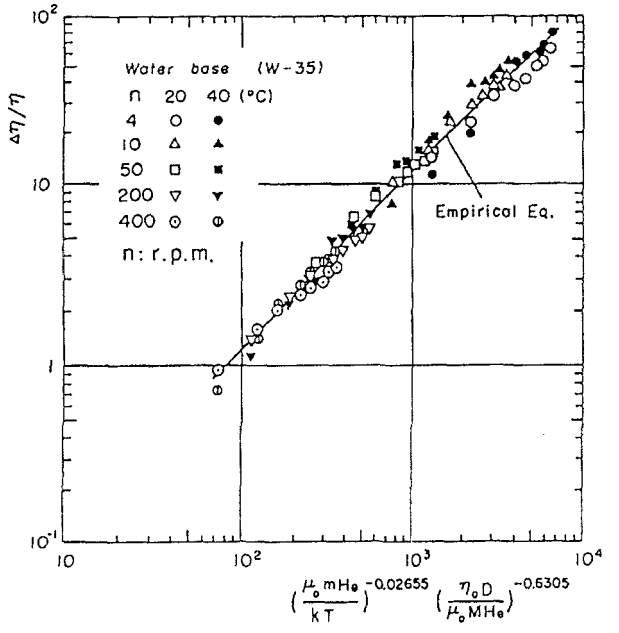

Figure 16: Magnetic field and shear rate dependence of the increase rate of apparent viscosity for water-based magnetic fluid.

As a result, experimental data on the pressure drop for the uniform field agree relatively well with predicted value for kerosene-based fluid. On the other hand, in the case of water-based fluid, the experimental values are much larger than the analytical prediction. Since it is observed that the large pressure drop also occurs at the non-uniform field region, it is important to examine the effect of nonuniform magnetic field on the flow resistance. Experimental work was also done to clarify the effect of nonuniform magnetic field on the flow resistance. The nonuniform magnetic field distribution was generated by adjusting the pole gap of the electromagnet as shown in Fig. 11, where the parameter I means the supplied current to the electromagnet. Fig. 12 shows the experimental results of the pressure change $\Delta p'_{1-2}$ against mean flow velocity at several I-values for both water-based and kerosene-based fluids. $\Delta p'$ denotes the pressure drop over the pipe length L:

$$\Delta p' = \lambda \frac{L}{d} \rho \frac{u_0^2}{2} . \tag{43}$$

In this case, subscript 1-2 denotes the change between the locations z_1 and z_2 in Fig. 11. The theoretical values obtained from Eq.(28), modified for the transverse magnetic field, are also shown in the same figure. The experimental values for the kerosene-based agree considerably well with the predicted ones as indicated in the figure. On the other hand, it is easy to see that the experimental values for the water-based fluid are much larger than the predicted ones. Fig. 13 shows the relation between the increasing rate of the resistance coefficicnt $(\Delta\lambda/\lambda)_{1-2}$ and Reynolds number Re. The increasing rate for the water-based fluid is nearly ten times as large as that for the kerosene-based fluid, which is similar to the pressure drop as indicated in Fig. 12. It is also clear that the effect of nonuniform magnetic field on the increasing rate of the resistance coefficient is more obvious at the lower velocity range.

The increase in the flow resistance due to the magnetic field is not thought to be independent of the rheological characteristics of magnetic fluids. Experimental studies were made to clarify the effects of magnetic field on the characteristics[13]. Measurements of the flow characteristics were made by means of the concentric-cylinder-type viscometer shown schematically in Fig. 14. It was improved so as to be able to operate in a strong magnetic field region. The tested magnetic fluids were water-based, hydrocarbon-based and diester-based fluids. A flow curve at liquid temperature of 20°C

is shown in Fig. 15 as an example of the experimental results. It is clearly indicated that each magnetic Auid in the case of no magnetic field shows the flow characteristics of a Newtonian Fluid: the shear stress increases linearly with the shear rate. Hydrocarbon-based fluids behave as Newtonian fluid, even in the case of applied magnetic field. However, water-based and diester-based fluids in the case of applied field show the pseudoplastic Auid: the increasing rate of apparent viscosity changes with apparent shear rate. In particular, it is clearly indicated that the viscosity of the water-based fluid increases extraordinarily due to the application of magnetic field at the region of small apparent shear rate. This increase is thought to be related closely to a peculiar pipe flow resistance in the case of the water-based magnetic fluid. The experimental result for the water-based magnetic Auid is shown in Fig. 16. It is indicated in the figure that the increasing rate of viscosity due to the magnetic field is extremely high in the region of small shear rate. The predicted value based on the approximate analysis in the case of $\Omega\tau_B \geq 1$ is considerably small compared with the measured value: the predicted value was of the order of $\Delta\eta/\eta < 10^{-1}$. Thus, the increment in apparent viscosity cannot be explained by the theory. It is believed that this peculiar characteristics of the water-based magnetic fluid have close relation to particles' aggregation or formation of cluster. To clarify the influence of clusters on the rheological propcrties of the water-based magnetic fluid, a theoretical analysis was carried out on the basis of the assumption that the particles in magnetic fluid form rigid linear aggregates to rnake a cluster[14]. The numerical results showed that the large increment of apparent viscosity occurs in the case of a magnetic field perpendicular to the shearing plane and that Non-Newtonian viscosity appears above a certain value of rotary Péclet number P_{er}. The mechanism of particles' aggregates has also been discussed. The phenomena in the water-based fluid is supposed to be caused by affinity of the surfactant for the solvent; that is, two kind of surfactant are used in the case of the water-based fluid. Two-dimensional computer simulations were also conducted by introducing the concept of a hydrophobic bond[15]. It was clarified that the problem concerning the particles' aggregation can be reasonably explained by this theory.

11.3 Unsteady **flow**

II.3.1 Pulsating **pipe** flow **characteristics**

The pulsating pipe Aow problem is also important in relation to the development in the application of oscillatory flow to magnetic Auid dampers and actuators. We consider here a pulsating pipe flow in steady and unsteady magnetic fields to solve the more generalized case of the basic Eqs. (14)-(16). When the basic equations are simplified by the same procedure **as** for steady flow in Section 11.2, the following dimensionless equation is obtained:

$$W^2\left(\frac{du^*}{dt^*}\right) = -\frac{dp'^*}{dz^*} + \left(1+\sin^2\$\,\frac{2\Delta\eta}{\eta}\right)\frac{d^2u^*}{dr^{*2}} + \left(1+\cos^2\theta\frac{2\Delta\eta}{\eta}\right)\frac{du^*}{r^*dr^*}\,, \tag{44}$$

together with the boundary conditions

$$r^* = 1: \quad u^* = 0; \quad r^* = 0: \quad du^*/dr^* = 0\,. \tag{45}$$

Here $W = r_0/\sqrt{\omega\rho/\eta}$ is Womersley number,

$$\left.\begin{aligned} p^{*\prime} &= p^* - \tfrac{nkT}{\eta\omega}\ln(\xi^{-1}\sinh\xi)\,, \\ \Delta\eta &= \tfrac{3}{4}\varphi\eta_0\tfrac{\xi-\tanh\xi}{\xi+\tanh\xi}, \varphi = \tfrac{3}{4}\pi a^3 n \end{aligned}\right\} \tag{46}$$

and also,

$$\left.\begin{aligned} &r^{*\prime} = r/r_0,\ z^* = z/r_0,\ u^* = u/\omega r_0 \\ &p^* = p/\eta\omega,\ t^* = \mathrm{wt} \end{aligned}\right\} \tag{47}$$

Eq. (44) is solved nurnerically by assuming that each time-varying variable is expanded in a series and ordering the resulting terms with respect to the powers of n[16]. Time-varying velocity profiles in a circular pipe are obtained as a function of the Womersley number W and the magnetic field parameter. Generally speaking,

it was clear from the numerical calculations for steady and unsteady magnetic field that the velocity profiles are mainly influenced by W as in to ordinary fluid flow; for smaller W, the velocity profile is parabolic-like and, for larger W, it becomes the profile having a maximum near the wall. Fig. 17 shows the velocity profile in the case of unsteady magnetic field as an example of the numerical results. In this case, the calculation was done under the assumption that the pressure gradient dp_n/dz^* and the magnetic field H_y are expressed as follows:

$$\left.\begin{aligned} dp_N/dz^* &= P_0 + P_1 \exp(it^*) \quad (P_0/P_1 = 2) \\ H_y(t^*) &= 140 + 100 \exp i(t^* - \beta)[kA/m] \end{aligned}\right\}$$

The curves in this figure represent the velocity profile at different instants; β denotes the phase difference between periodic pressure and magnetic field fluctuation. It is easy to see that the profile is also affected by the phase difference β although it mainly changes due to the Womersley number W.

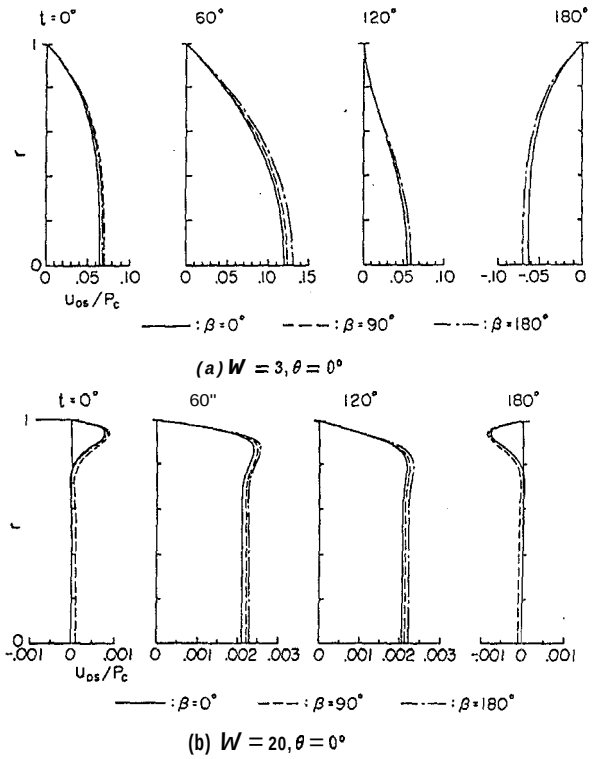

Figure 17: Velocity profile in an oscillatory pipe flow.

II.5.2 Oscillating flow (experimental study)

Experimental study of an oscillating pipe flow with constant amplitude in a steady magnetic field is carried out using a experimental apparatus as sketched in Fig. 18; the oscillatory flow of magnetic fluid is produced through the piston **(3)** by the vibration exciter (1), and a nonuniform magnetic field whose gradient is steep is applied to the magnetic fluid flow transversely to the pipe axis by an electromagnet (5)[16]. The pressure variation was measured by means of the pressure transducers (4) placed at the upper and lower positions outside the electromagnet. In this study, the effect of the applied field on the pressure difference Ap and phase difference β between the upper and lower locations is examined. Since large pressure drop occurs in the nonuniform magnetic field region in the case of water-based magnetic fluid, water-based magnetic fluid was employed in this experiment. Also, electromagnet was designed so that the steep magnetic field gradient is realized. Fig. 19 shows the magnetic field distribution on the centerline of the pipe axis.

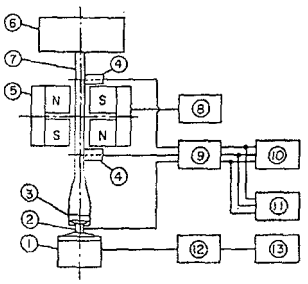

①Vibration exciter, ②Impedance head, ③Piston, ④Pressure transducer, ⑤Electromagnet, ⑥Reservoir, ⑦Circular pipe, ⑧D.C. power supply, ⑨D.C. power amplifier, ⑩Spectrum analyzer, ⑪Oscilloscope, ⑫D.C. power amplifier, ⑬Function generator

Figure 18: Scheme of experimental apparatus of oscillatory pipe flow.

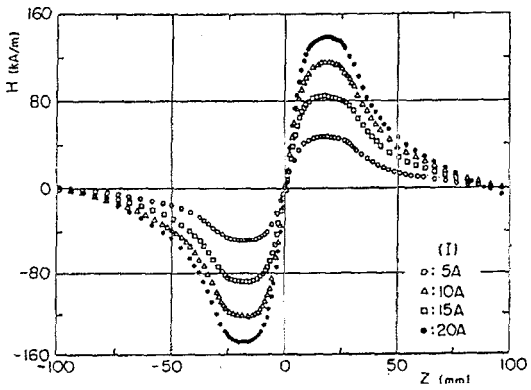

Figure 19: Magnetic field distribution in the case of oscillatory pipe flow.

Theoretical analysis of the oscillatory flow was also made under the assumption that the shape of aggregated particles in a magnetic fluid is an elongated ellipsoid as sketched in Fig. 20[17]. Fig. 21 indicates the

rate of the increase in the pressure difference due to the imposed magnetic field $(\Delta\bar{p}^*_{20(A)} - \Delta\bar{p}^*_{0(A)})/\Delta\bar{p}^*_{0(A)}$ as a function of the Womersley number W. Here Nu denotes the number of the aggregated particles. It is clear that the increasing rate of the pressure difference due to the application of nonuniform magnetic field becomes larger with increase in the number of the particles Nu. The pressure difference also shows large value at low W. Experimental data plotted in the figure indicate that the pressure difference due to the nonuniform field increases with decrease in W, too. Since the predicted results of the pressure difference show the same tendency as the experimental data, the experimental data could be qualitatively explained by the theoretical analysis based on the consideration of the aggregate of magnetic particles.

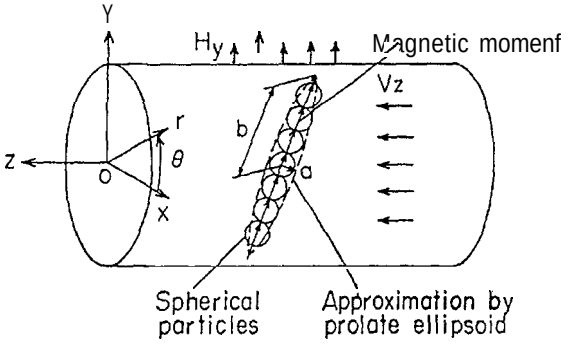

Figure 20: Model of aggregated particles in a magnetic field.

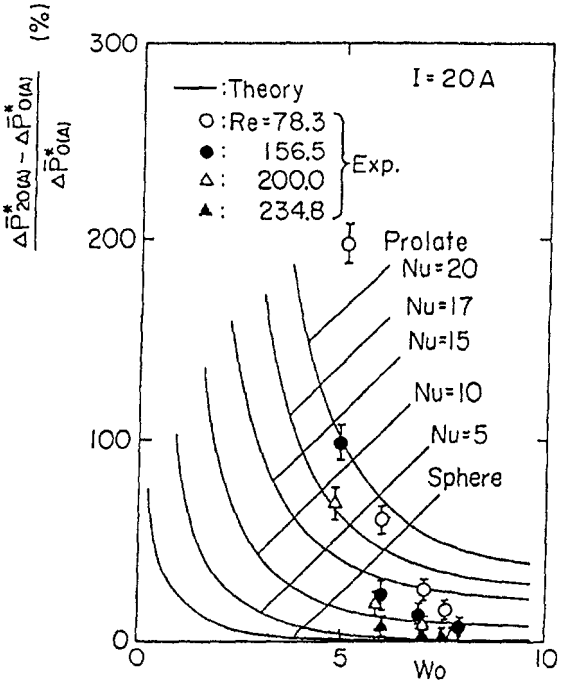

Figure **21:** Increase rate of pressure difference versus Wormersley number.

II.3.3 Flow induced by alternating magnetic field

The oscillation of a magnetic fluid column, that is, a magnetic fluid plug, has been studied for developing a magnetic fluid plug actuator[18,19]. Let us consider the oscillatory Aow in a U-shaped tube as sketched in Fig. 22; magnetic fluid and nonmagnetic fluid are held in the tube. The length of each fluid column is l_m for magnetic fluid and l_f for nonmagnetic fluid. The magnetic fluid plug is supported by non-uniform static magnetic field. z_{20} represents the initial height from the upper interface of the plug to the center of the applied field. The oscillatory motion of the magnetic fluid plug is induced by applying harmonic oscillations to the magnetic field, which drives the oscillating flow of nonmagnetic liquid. Assuming that each flow is laminar, the pipe friction coefficients can be estimated as $\lambda_i = 64/Re_i$, where $Re_j = \rho_i v d/\eta_i$ and i = f,m. The governing equation for this oscillating flow can be expressed as:

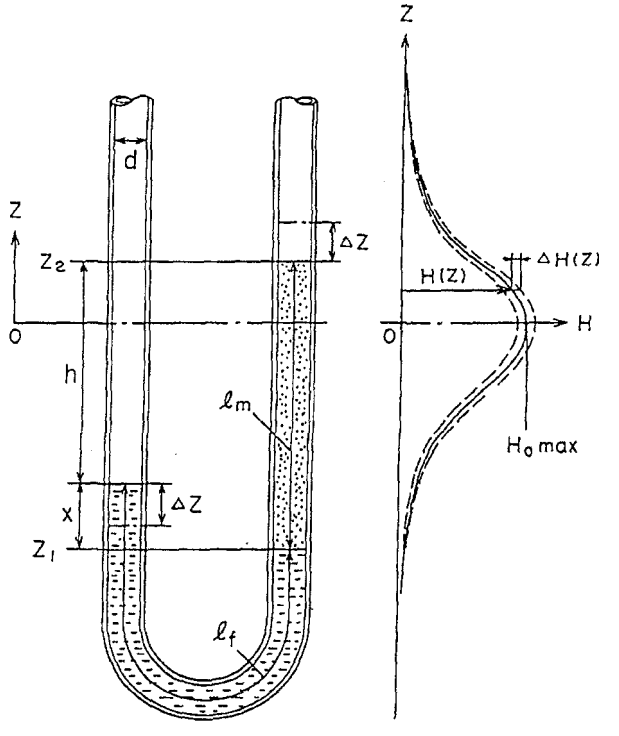

Figure **22:** Oscillatory motion of magnetic fluid plug in an U-shaped tube.

$$(\rho_f l_f + \rho_m l_m)\frac{d^2\Delta z}{dt^2} + \frac{32\eta_m}{d^2}\left\{\gamma\left(l_f + \zeta_f \frac{Re_f d}{64}\right) + \left(l_m + \zeta_m \frac{Re_m d}{64}\right)\right\}\frac{d\Delta z}{dt}$$
$$+ g\rho_m l_m + \rho_f(l_m - h - 2\Delta z) - \mu_0 \int_{H_1}^{H_2} M dH = 0 \ , \tag{48}$$

where $\gamma = \eta_f/\eta_m$ and ζ denotes the loss coefficient. Also, subscript f and m denotes the nonmagnetic liquid and the magnetic fluid, respectively. Applying the Langevin function, $M = nmL(\xi)$, to the magnetization M, where $L(\xi) = coth\xi - \xi^{-1}$ and $\xi = \mu_0 mH/kT$ and introducing d and $\sqrt{d/g}$ as representatives of length and time to make the equation dimensionless Eq.(48) can be written as

$$\frac{\mathrm{d}^2\mathrm{Az}^*}{\mathrm{dt}^*} + 2\alpha_1 \frac{d\Delta z^*}{\mathrm{dt}^*} + \frac{l_m^*(1-\rho_f^*) + \rho_f^*(\mathrm{h}^* + 2\Delta z^*)}{(\rho_f^* l_f^* + l_m^*)} - \alpha_2 \ln \frac{\xi_1 \sinh \xi_2}{\epsilon_2 \sinh \epsilon_1} = 0 \ , \tag{49}$$

where

$$\left.\begin{aligned} &\alpha_1 = \frac{16Fr}{Re_m}\frac{\gamma l_f^* + l_m^* + (\gamma\zeta_f Re_f + \zeta_m Re_m)/64}{\rho_f^* l_f^* + l_m^*} \ , \\ &\text{in which } \mathrm{Fr} = v/\sqrt{dg} \\ &\alpha_2 = \frac{nkT}{\rho_m g d(\rho_f^* l_f^* + l_m^*)} \ , \end{aligned}\right\} \tag{50}$$

The, superscript * denotes dimensionless quantities.

Assuming the initial condition $\mathrm{t}^* = 0$, $\mathrm{Az}^* = 0$, linearizing Eq.(49) and, for simplicity, representing Δz^* by z^*, the resultant equation can be expressed as

$$\frac{\mathrm{d}^2\mathrm{z}^*}{dt^{*2}} + 2\alpha_1 \frac{\mathrm{dz}^*}{\mathrm{dt}^*} + \alpha_1 \chi z^* = \mathrm{F}\sin\mathrm{wt}^* \tag{51}$$

Here,

$$\left.\begin{aligned} &\xi_1 \gg 1 : \\ &\chi = \frac{2\rho_f^*}{(\rho_f^* l_f^* + l_m^*)\alpha_2} + \left(\frac{d\xi}{dz^*}\right)_1 (1 - \xi_{10}^{1}) - \left(\frac{d\xi}{dz^*}\right)_2 (1 - \xi_{20}^{-1}), \\ &F = \alpha_2 \Delta\xi_1(\xi_{10}^{-1} - 1) - \Delta\xi_2(\xi_{20}^{-1} - 1) \ ; \\ &\xi_1 < 1 : \\ &\chi = \frac{2\rho_f^*}{(\rho_f^* l_f^* + l_m^*)\alpha_2} - \left(\frac{d\xi}{dz^*}\right)_2 (1 - \xi_{20}^{-1}) \ , \\ &\mathrm{F} = \alpha_2 - \Delta\xi_2(\xi_{20}^{-1} - 1) \ . \end{aligned}\right\} \tag{52}$$

A general solution of Eq.(51) can be easily obtained. After a sufficient long period, it reduces to

$$z^* = A\sin(\omega t^* - \delta) \ . \tag{53}$$

Here

$$\left.\begin{aligned} A &= F/\sqrt{(p^2 - \omega^2)^2 + 4\alpha_1^2\omega^2} \\ &= (F/p^2)/\sqrt{\{1 - (\omega^2/p^2)\}^2 + \{2\sigma(\omega/p)\}^2} \\ \delta &= \arctan[2\alpha_1\omega/(p^2 - \omega^2)] \\ &= \arctan[2\sigma(\omega/p)/\{1 - (\omega/p)^2\}] \\ p &= \sqrt{\alpha_2 \xi} \end{aligned}\right\} \tag{54}$$

and σ is the damping coefficient.

An experimental study is also carried out using the U-tube configuration where the motion of magnetic fluid plug is transferred to the piston supported by the spring through the nonmagnetic fiuid. Experimental apparatus and measuring devices are schematically shown in Fig. 23. A kerosene-based magnetic fluid of 20% mass concentration is used as the magnetic fluid plug and distilled water is employed as nonmagnetic liquid. Nonuniform static magnetic field for supporting the plug is produced by a constant supply current to electromagnet. Vertical position of the tube is adjusted to the position where z_{20} became a specified value. When a harmonically oscillating current is applied to the magnet, pulsating magnetic field is generated and added to the static field. Then, the oscillating flow is driven by the pulsating field. Displacement of the piston (9) is observed by means of the optical measuring system composed of displacement analyzer (7), digital storage oscilloscope (8) and camera. The amplitude of piston displacement as a function of frequency of the alternating field is obtained as various spring constant k_c as shown in Fig. 24. The maximum field strength in the stationary state is $H_{0max} = 26.5kA/m$, and the maximum amplitude of the alternating field is $\Delta H_{max} = 26.0kA/m$.

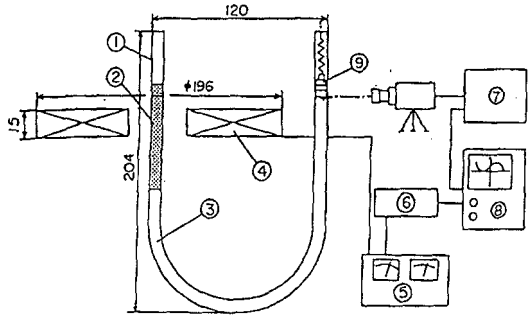

Figure 23: Scheme of experimental apparatus of magnetic fluid actuator.

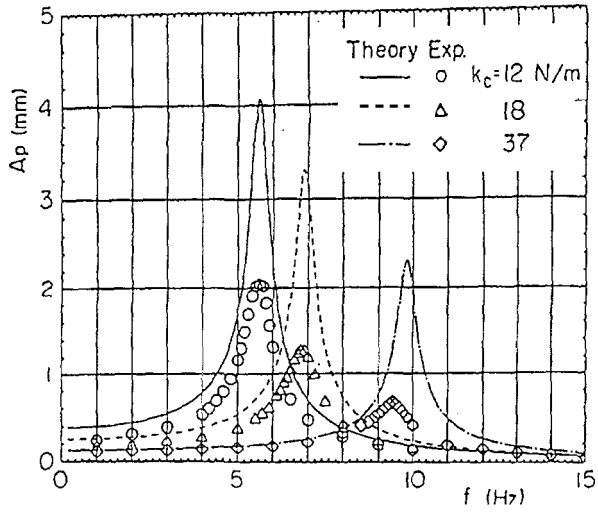

Figure 24: Effect of the spring constant k_c on the frequency response curve.

The analytical results[19] are also shown in Fig. 24. The theoretically predicted values are higher than the experimental values because the friction loss of piston was neglected in the analysis. However, they agree qualitatively.

11.4 Gas-liquid two-phase flow

Recently, a new energy conversion system utilizing gas-liquid two-phase flow of rnagnetic fluid has been proposed[20–22]. The system is based on the principle that the magnetization of the magnetic fluid changes with void fraction. It is well known that there is a similar proposal using a temperature-sensitive magnetic fluid. However, significant results have not been obtained since the magnetic Auid of satisfactory temperature-sensitivity have not been prepared. The above-mentioned new system can produce larger force since the properties of magnetization changes by gas inclusion as well as the temperature rise. Let us consider the one-dimensional two phase flow in the vertical pipe. Fig. 25 shows schematically the system used in the theoretical analysis as well as the experiment. The magnetic field H has nonuniform distribution along the z-axis. The magnetic fluid downstream, past that point of maximum field strength, is heated, as sketched in Fig. 25. Γ_g is the rate of vapor bubble production. In the experimental study, the vaporization by heat addition is replaced by air injection at $z = Q$ To simplify

the theoretical consideration, it is also assumed that the momentum equation of gas phase is represented by the motion of a single gas bubble. Under these assumptions, the governing equations can be written as follows[23]: the continuity for the gas phase is

$$\frac{d}{dz}(\rho_g v_g \alpha A) = \Gamma_g \tag{55}$$

and for the liquid phase

$$\frac{d}{dz}\{(\rho_l v_l (1-\alpha)A)\} = -\Gamma_g \ , \tag{56}$$

$$\Gamma_g = \frac{4}{3}\pi r_{min}^3 \rho_g N_g \ ,$$
$$N_g = \frac{n_{ga}}{\sqrt{2\pi\sigma}} \exp\left\{\frac{-(z-z_{max})^2}{2\sigma^2}\right\} \ , \tag{57}$$

where N_g the number of vapor bubble generation, n_{ga} is total number of bubble generation, r_{min} the minimum bubble radius, ρ_g the gas density and σ the variance.

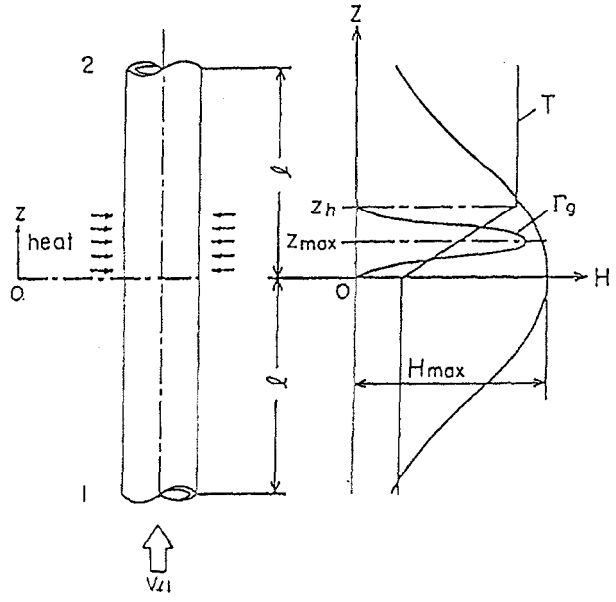

Figure 25: Analytical model of two-phase flow in a nonuniform magnetic field.

If viscosity effects are not taken into account, the combined momentum equation is

$$\frac{1}{A}\frac{d}{dz}\{\rho_g \alpha v_g^2 A + \rho_l (1-\alpha) v_l^2 A\}$$
$$= -\frac{dp_l}{dz} - (1-\alpha)\rho_l g + (1-\alpha)\mu_0 M \frac{dH}{dz} \ , \tag{58}$$

the momentum equation of the gas phase is

$$\frac{4}{3}\pi R^3 \rho_g v_g \frac{dv_g}{dz} =$$
$$= -\frac{4}{3}\pi R^3 \frac{dp_l}{dz} - -\frac{4}{3}\pi R^3 \rho_g g - F_D - F_{vm} \ , \tag{59}$$

the cornbined energy equation is

$$\frac{1}{A}\frac{d}{dz}\left\{\rho_g \alpha A v_g \left(h_g + \frac{v_g^2}{2}\right) + \rho_l (1-\alpha) A v_l \left(h_l + \frac{v_l^2}{2}\right)\right\}$$
$$= -\rho_l (1-\alpha) v_l g - (1-\alpha)\mu_0 T \left(\frac{\partial M}{\partial T}\right)_H v_l \frac{dH}{dz} + Q \ , \tag{60}$$

the equation of the state for the gas is

$$p_q/\rho_q = \mathcal{R}_G T \tag{61}$$

and the equation of contraction and expansion of the bubble is

$$Rv^2 \frac{d^2 R}{dz2} + Rv_g \left(\frac{dv_g}{dz}\right)\left(\frac{dR}{dz}\right) + \frac{3}{2}v_g^2 \left(\frac{dR}{dz}\right)^2 = \frac{1}{\rho_l}\left\{p_g - p_l - \frac{2\sigma}{R} - \frac{4\eta}{R} v_g \frac{dR}{dz}\right\} \ . \tag{62}$$

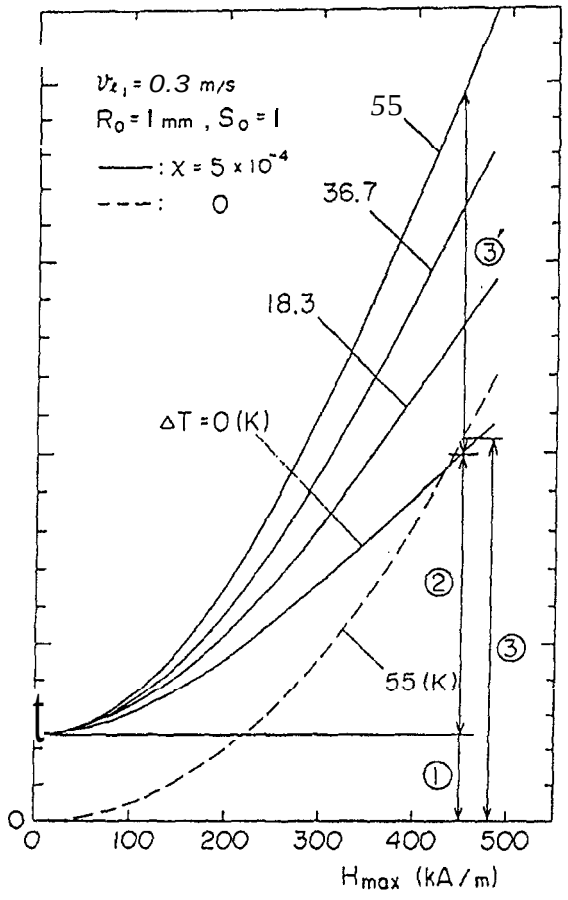

Figure 26: Numerical example of pressure rise owing to the gas injection as a function of maximum magnetic field strength.

Here A is the cross-sectional area of the pipe, F_D the drag force, F_{vm} the virtual mass force, $\mathcal{R}_G$ the gas constant, R the bubble radius, Q the heat added to fluid per unit volume through pipe wall, v fluid velocity, α the void fraction and ρ the density. Also, subscripts g and l denote gas phase and liquid phase, respectively. We can obtain the flow characteristics by solving simultaneously Eqs. (55)-(62). It is shown that the injection of gas bubbles in the throat increases the pressure rise in diverging duct under a nonuniform magnetic field[20]. The calculated results were confirmed by an experimental study. Moreover, theoretical and experimental studies were made to clarify the effect of magnetic field on the two-phase flow characteristics of a temperature-sensitive magnetic fluid.

Fig. 26 shows a typical example of the numerical results concerning the effect of magnetic field on the pressure rise owing to the gas injection[21]. It is clear that the pressure rise for gas injection is considerably large compared with that for no gas injection; for example, in the case of AT = 55°C, part (1) corresponds to the pressure rise caused by the effect of air lift pump, (2) by the effect of gas injection on rnagnetization reduction, and (3) and (3)' by the effect of heating on magnetization reduction. Fig. 27 shows the pressure difference Δp_{lm} due to heating for three cases of air flow rate Q_g in the case of a bubble radius $R_0 = 1$ mm at the injection point[22]. Here, AT is the temperature difference between the entrance and the exit of the magnetic field region. Experimental results, under similar conditions to the theoretical analysis, are also plotted in this figure. In the experiment, Ferricolloid TS-50K (Taiho Industries Co.), which has a 50% mass concentration of Mn-Zn ferrite particles, was used as the temperature- sensitive magnetic fluid. The pressure difference Δp_{lm} indicates the pressure increase at the exit of the field region due to magnetic force only, compared to the single phase flow in a magnetic field. It is obviously known that the driving force becomes larger by injecting air into the magnetic fluid.

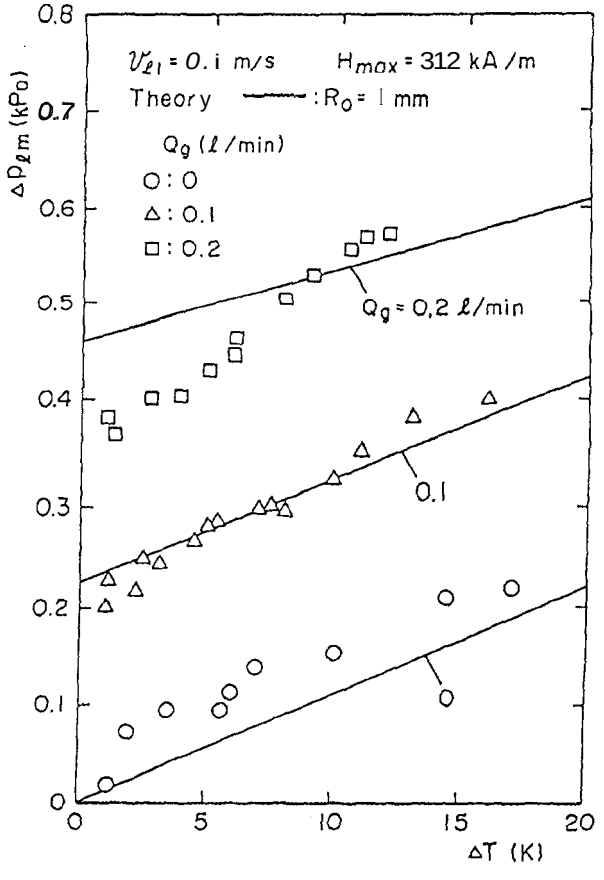

Figure 27: Presure rise due to heating and air injection for the case of air flow rate Q_g.

III. Conclusion

This review deals with the recent research works of hydrodynamics of magnetic fluids, especially various pipe flow problems conducted mainly in Japan.

Firstly, the effect of uniform and nonuniform magnetic field on the pipe flow resistance is investigated. Several experimental studies show that a large increase of flow resistance is induced by the application of magnetic field. The large increase in the apparent viscosity is also obtained due to the applied magnetic field in the measurement of rheological characteristrics of magnetic fluid using concentric cylinder type viscometer.

These experimental data suggest that the small particles in a strong magnetic fielcl partially aggregate to form a chain like cluster. Therefore, an analytical model of particle aggregate is considered in the oscillatory pipe flow case and compared with the experimental data.

As a specific example of pipe flows, an oscillastory motion of a magnetic fluid plug induced by an oscillating magnetic field is investigated as the basis for the development of magnetic fluid actuators.

Finally, gas-liquid two-phase flow is investigated theoretically and experimentally for the development of a new energy conversion system by using magnetic fluid.

References

1. L. D. Landau, E. M. Lifshitz and L. P. Pitaevskii, *Electrodynamics of Continuous* Media, (Pergamon Press, 1984) p.127.
2. J. L. Neuringer and R. E. Rosensweig, Phys. Fluids, 7-12, 1927 (1964).
3. M. I. Shliomis, Sov. Phys. JETP, 34-6, 1291 (1972).
4. I. G. Shaposhnilrov and M. I. Shliomis, Magn. Gidro., (in Russian), **1**, 47 (1975).
5. S. Kamiyama, K. Koike and N. Iizuka, Trans. Jpn. Soc. Mech. Eng., (in Japanese), 45-400, B, 1843 (1979); S. Kamiyama, K. Koike and N. Iizuka, Rep. Inst. High Speed Mech., Tohoku Univ., 41-323, 21 (1980).
6. S. Kamiyama, K. Koike and N. Iizuka, Trans. Jpn. Soc. Mech. Eng., (in Japanese), 45-389, B, 37 (1979); S. Kamiyama, K. Koike and N. Iizuka, Bull. JSME, 22-171, 1205 (1979).
7. S. Kamiyama and K. Mokuya, Trans. Jpn. Soc. Mech. Eng., (in Japanese), **47-424**,B, 2290 (1981); S. Kamiyama and K. Mokuya, Magn. Gidro., (in Russian), No.**1**, 18 (1982).
8. J. P. McTague, J. Chem. Phys., 51-1, 133 (1969).
9. S. Kamiyama, T. Oyama and K. Mokuya, Trans. Jpn. Soc. Mech. Eng., (in Japanese), 47-424, B, 2299 (1981).
10. S. Kamiyama, K. Koilre and T. Oyama, J. Magn. Magn. Mat., 39- 1&2, 23 (1983).
11. S. Kamiyama, K. Koike and T. Oyama, Mem. Inst. High Speed Mech., 54-448, 41 (1985).
12. S. Kamiyarna, J. Htwe, K. Koike and T. Oyama, J. Magn. Magn. Mat., **65**-2&3, 317 (1987).
13. S. Kamiyama, K. Koike and Z-S. Wang, Trans. Jpn. Soc. Mech. Eng., (in Japanese), **52-484**, B, 3947 (1986); S. Kamiyama, K. Koike and Z-S. Wang, JSME Int. J., 30-263, B, 761 (1987).
14. S. Kamiyama and A. Sato, J. Colloid Interface Sci., 127-1, 173 (1989).
15. A. Sato and S. Kamiyama, *Continuum* Mechanics and its *applications*, edited by G. A. C. Graham and S. K. Malik, (Hemisphere Publ., 1989) Vol.1, pp.731.
16. S. Kamiyama, K. Koike and Y. Ikeda, Trans. Jpn. Soc. Mech. Eng., (in Japanese), 54-508, B, 3331 (1988).
17. S. Kamiyama and K. Shimada, Proc. 2nd KSME-JSME Fluids Eng. Conf., (1990), Vol.2, pp.299.
18. A. Sato, T. Oyama, K. Koike and S. Kamiyarna, Trans. Jpn. Soc. Mech. Eng., (in Japanese), 57-534, B, 520 (1991).
19. S. Kamiyama, J. Watanabe and A. Sato, Trans. Jpn. Soc. Mech. Eng., (in Japanese), 57-537, B, 1623 (1991).
20. S. Kamiyama and S. Inoue, Trans. Jpn. Soc. Mech. Eng., (in Japanese), 54-497, B, 80 (1988).
21. H. Ishikawa, K. Koike, S. Kamiyamaand S. Inoue, Mem. Inst. High Speed Mech., Tohoku Univ., (in Japanese), 60-483, **1** (1988).
22. S. Kamiyama and H. Ishikawa, Trans. Jpn. Soc. Mech. Eng., (in Japanese), 55-511, B, 741 (1989).
23. S. Kamiyama and M. Okubo, Proc. Int. Symp. on Multi-Phase Flows, Tsukuba, (1991), pp.77.